Structural Analysis of Al, Ni, and Cu Using the Maximum Entropy Method, Multipole and Pair Distribution Function

Muthaian Charles Robert[a], Ramachandran Saravanan[b], Krishnamoorthy Saravanakumar[c], and Murugesan Prema Rani[b]

[a] Department of Physics, H.K.R.H. College, Uthamapalayam – 625 533, Tamil Nadu, India
[b] Department of Physics, The Madura College, Madurai – 625 011, Tamil Nadu, India
[c] Madurai Kamaraj University, Madurai – 625 021, Tamil Nadu, India

Reprint requests to Dr. R. S.; E-mail: saragow@dataone.in

Z. Naturforsch. **64a,** 361 – 369 (2009); received November 13, 2007 / revised July 23, 2008

The average and local structures of the metals Al, Ni, and Cu have been elucidated for the first time using the MEM (maximum entropy method), multipole and PDF (pair distribution function). The bonding between the constituent atoms in all these systems is found to be well pronounced and clearly seen from the electron density maps. The MEM maps of all three systems show the spherical core nature of the atoms. The mid bond electron density profiles of Al, Ni, and Cu reveal the metallic nature of the bonding. The local structure using the PDF profile of Ni is compared with that of previously reported results. The R value in the present work using low Q XRD data for the PDF analysis of Ni is close to the value in the literature using high Q synchrotron data. The cell parameters and displacement parameters are also studied and compared with the reported values.

Key words: Metals; Rietveld; Maximum Entropy Method; Pair Distribution Function; Multipole; Local Structure.

1. Introduction

Today's technological evolution results in efforts to produce new and sophisticated materials of immense use in domestic, technical, and industrial applications. Usually, the synthesis of new materials results in single-phase materials, though often not in single-crystalline form. Hence, a complete analysis of the structure, the local distribution of atoms, and the electron distribution in the core, the valence and the bonding region is necessary using powder diffraction methods, since most of the recent materials are initially obtained in powder form. Since one makes efforts to produce single crystals from powders, a prior analysis is required using powders to proceed with single crystal growth.

In this context, we have considered the three metals Al, Ni, and Cu and have collected powder data sets, to study the structure in terms of the local and average structural properties using the pair distribution function (PDF), the electron density distribution between atoms using the maximum entropy method (MEM), and the bonding of the core and the valence electron distribution using multipole techniques. Particularly, the PDF analysis requires data sets up to very high values of Q ($= 4\pi \sin\theta/\lambda$) achievable only through synchrotron studies, which are not always accessible. But the present work gives reasonable results, which could be obtained through single-crystal work or through high Q data sets, only using powder samples in laboratory experiments. Also, a study on the electronic structure of the metals using the most versatile techniques like MEM [1] and the multipole method [2], being available today, was carried out. If the tools available for the analysis yield highly precise information, it is appropriate to apply them to available precise data sets, as has been done in the present work, thereby the methodology can also be tested.

In order to elucidate the distribution of valence electrons and the contraction/expansion of atomic shells, a multipole analysis of the electron densities has been carried out using the software package JANA2000 [3]. Recently, the multipole analysis of the charge densities and bonding has been widely used to study the electronic structure of materials [4 – 8]. In the present work, the multipole model proposed by Hansen and Coppens [2] has been used for elucidating the electronic structure.

2. Data Collection and Structural Refinement

The powder X-ray intensity data were collected at Regional Research Laboratory (RRL), Council of

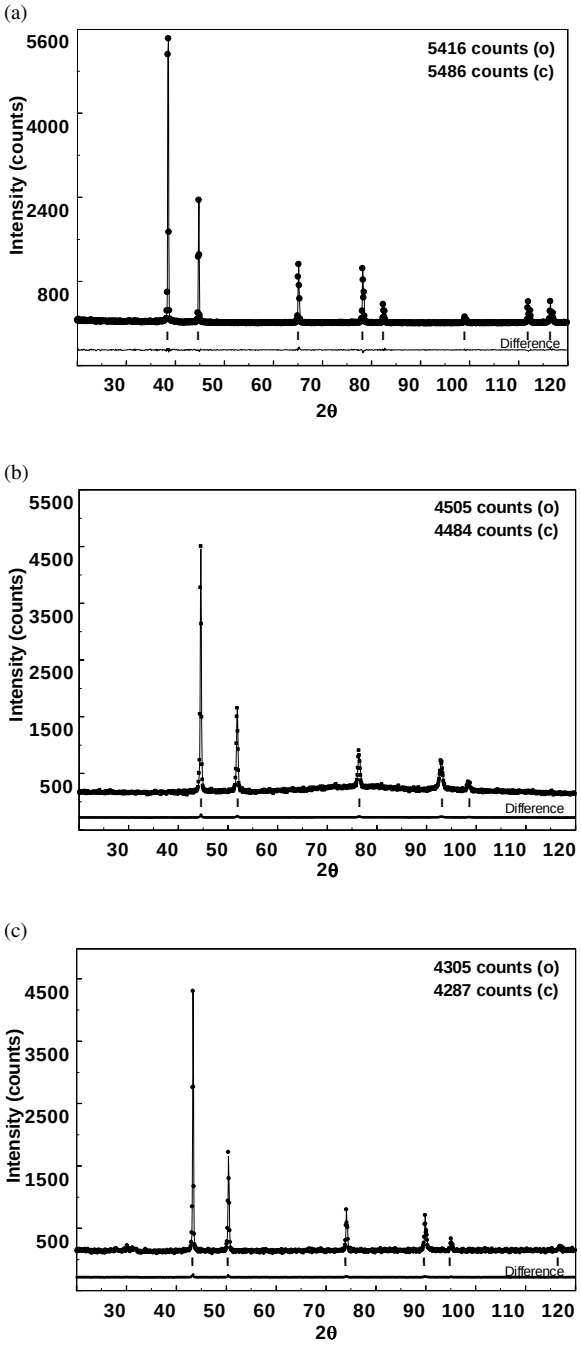

Fig. 1. (a) The JANA refinement profile together with the difference between the observed and calculated relative intensities for Al. (b) The JANA refinement profile together with the difference between the observed and calculated relative intensities for Ni. (c) The JANA refinement profile together with the difference between the observed and calculated relative intensities for Cu.

Table 1. The refined structural parameters using JANA2000.

Parameter	Al	Ni	Cu
Cell parameter (nm)	0.405210(4)	0.352660(7)	0.362540(5)
Cell parameter (nm) [22]	0.40495	0.35238	0.36149
B (10^{-2} nm^2)	0.983(80)	0.561(64)	0.432(53)
B (10^{-2} nm^2) [21]	0.746	0.3401	0.526
R_P (%)	9.84	6.21	6.77
wR_P (%)	6.23	7.88	8.63

Table 2. Observed and calculated structure factors for Al.

h	k	l	F_o	F_c	$F_o - F_c$	$\sigma(F_o)$
1	1	1	35.0717	35.0451	0.0266	0.2199
0	0	2	32.8710	32.8386	0.0324	0.1555
2	0	2	26.6339	26.8235	−0.1896	0.3569
1	1	3	22.8654	23.1844	−0.3190	0.1095
2	2	2	22.3412	22.1719	0.1693	0.5815
0	0	4	18.8339	18.6439	0.1900	0.8294
3	1	3	15.9612	16.4700	−0.5089	0.2220
2	0	4	16.2283	15.8219	0.4064	0.3717

Table 3. Observed and calculated structure factors for Ni.

h	k	l	F_o	F_c	$F_o - F_c$	$\sigma(F_o)$
1	1	1	68.1582	67.9282	0.2300	0.4201
0	0	2	61.3964	61.9646	−0.5682	0.5924
2	0	2	44.3751	45.7638	−1.3888	0.6798
1	1	3	38.5964	37.5945	1.0020	0.5607
2	2	2	34.0123	35.3752	−1.3629	1.3103

Table 4. Observed and calculated structure factors for Cu.

h	k	l	F_o	F_c	$F_o - F_c$	$\sigma(F_o)$
1	1	1	78.5875	78.4925	0.0950	0.5324
0	0	2	72.7074	72.6464	0.0610	0.7634
2	0	2	55.3407	55.4621	−0.1214	0.8717
1	1	3	46.9975	46.7284	0.2690	0.7452
2	2	2	44.0637	44.3322	−0.2685	1.6701
0	0	4	35.9465	36.5819	−0.6354	2.9896

Scientific and Industrial Research (CSIR), Thiruvananthapuram, India, using an X-PERT PRO (Philips, Netherlands) X-ray diffractometer with a monochromatic incident beam, which offers pure Cu Kα_1 radiation. The wavelength used for the X-ray intensity data collection was 0.154056 nm with a 2θ range of data collection from 10° to 120°. The raw intensities were refined using the software program JANA2000 [3], considering the fcc unit cell of Al, Ni, and Cu with 4 atoms/unit cell in the space group $Fm\bar{3}m$. The fitted profiles of the observed and calculated relative intensities with the Bragg peaks together with their difference are given in Figs. 1a – c for Al, Ni, and Cu, respectively. The results of the refinements are given in Table 1. The refined structure factors are given in Tables 2, 3, and 4, respectively, for Al, Ni, and Cu.

System	Prior ED[a] (10^{-3} e/nm^3)	Resolution (nm/pixel)	λ	R_{MEM} (%)	wR_{MEM} (%)	Number of of cycles
Al	0.7806	0.00633	0.010	1.3839	0.7897	1685
Ni	2.5538	0.00551	0.015	1.2011	1.0346	830
Cu	2.4344	0.00567	0.005	1.7610	1.2318	1072

Table 5. Parameters of the MEM refinement.

[a] ED, electron density.

Table 6. Electron density profiles along the three directions of the unit cells.

Direction	[100]		[110]		[111]	
System	Position (nm)	ED[a] (10^{-3} e/nm^3)	Position (nm)	ED[a] (10^{-3} e/nm^3)	Position (nm)	ED[a] (10^{-3} e/nm^3)
Al	0.2026	0.1467	0.1433	0.2636	0.3509	0.1467
Ni	0.1763	0.2296	0.1247	1.1010	0.3054	0.2296
Cu	0.1813	0.3318	0.1282	0.7649	0.3139	0.3317

[a] ED, electron density.

2.1. MEM Refinements

The refined structure factors were used for the MEM analysis by the methods discussed in earlier works, e. g., by Saravanan et al. [9] and Israel et al. [10 – 12]. In the present calculation, the unit cell was divided into 64^3 pixels and the initial electron density at each pixel was fixed uniformly as Z/a_0^3, where Z is the number of electrons in the unit cell. The electron density was evaluated by carefully selecting the Lagrange multiplier in each case such that the convergence criterion C became unity after performing a minimum number of iterations. The resulting parameters of the MEM computations are given in Table 5.

The electron density distribution of Al, Ni, and Cu has been mapped using the MEM electron density values obtained through refinements. Figures 2a – c show the MEM electron density distribution of Al, Ni, and Cu in the (100) plane of the unit cell. Figures 2d – f show the MEM electron density distribution of Al, Ni, and Cu in the (110) plane. Figures 3a – c show the one-dimensional variation of the electron densities of Al, Ni, and Cu along the three directions [100], [110] and [111] of the unit cell, respectively. The electron densities at the saddle points along these three directions are presented in Table 6. A detailed discussion is given in the next section based on these two-dimensional MEM maps and one-dimensional profiles.

2.2. PDF Refinements

For materials whose structure is not reflected in the long-range order of the crystal, an alternative structural analysis, called the pair distribution function (PDF) approach, is used. This method is sometimes called the real-space structure determination method, because the PDF is modeled in real space rather than in the reciprocal space. The PDF reflects preferentially the short-range ordering in a material. It is defined as the probability to find an atom at a distance r from another atom. In other words the PDF gives the bond length distribution of the material under consideration [13]. The PDF agrees well with the interatomic distances computed from a crystallographic model, when there are no short-range deviations from the average structure [14, 15].

Table 7. Distances from the PDF profiles.

System	First nearest neighbour distance (nm)	
	Observed	Calculated [22]
Al	0.286	0.2863
Ni	0.250	0.2492
Cu	0.238	0.2564

This approach has been used for studying the structure of glasses and liquids [16 – 18]. More recently, it has been applied to disordered crystalline and to partially crystallized materials. Quantitative structural information on nanometer length scales can be obtained by fitting a model directly to the PDF [19] based on the equation

$$G(r) = 4\pi r[\rho(r) - \rho_0] = \frac{2}{\pi}\int \vec{Q}[S(\vec{Q}) - 1]\sin(\vec{Q}r)\mathrm{d}\vec{Q},$$

where $G(r)$ is the atomic pair distribution function and $\rho(r)$ corresponds to the (atomic) number density at a distance r from the average atom. The atomic pair distribution function, obtained from powder diffraction data, thus is a valuable tool for the study of the local atomic arrangements in a material, since both Bragg and diffuse scattering information about local arrangements are preserved in the PDF.

In the present study, the observed PDFs of Al, Ni, and Cu were obtained from the raw intensity data us-

Table 8. Parameters from multipole refinement.

Parameters	Al	Ni	Cu
κ'	1.006926(0.052132)	1.1132(0.01367)	1.064866(0.34471)
B (10^{-2} nm^2)	0.9831(0.0809)	0.56048(0.0640)	0.43179(0.0533)
R (%)	0.84	2.12	0.59
wR (%)	1.2	1.61	0.36
GoF	1.16	1.16	1.09
$\rho_{\max\,(\mathrm{SMD})}$	0.05	0.02	0.02
$\rho_{\min\,(\mathrm{SMD})}$	−0.02	−0.08	−0.01

ing the software program PDFgetX [20] after performing corrections such as the multiple scattering correction, polarization correction, absorption correction, normalization correction and Compton correction. A comparison between the observed and calculated PDFs has been carried out using the software package PDFFIT [19]. Figures 4a – c give the observed and calculated PDF profiles together with the difference between them for Al, Ni, and Cu, respectively, and Table 7 gives the bond length distribution of the atoms.

2.3. Multipole Refinements

The multipole model represents an extrapolation from a finite set of experimental data. An important feature of the multipole model is the possibility to adjust the radial dependence for each atom type by including the expansion-/contraction-controlling parameters κ' in the refinement, and possibly also the parameters κ'', to change the radial dependence of the valence deformation density.

In our study, we have used a modified electron density model proposed by Hansen and Coppens [2] with the option that allows the refinement of population parameters at various orbital levels, multipoles up to seventh order and corresponding radial expansion (κ') parameters. The κ' parameters were refined in separate cycles together only with the scale factor, and convergence was achieved in an iterative process. Each refinement cycle was considered successful at the point at which the maximum shift/s. u. was less than 0.001. The parameters and results obtained from multipole refinements are given in Table 8.

The effect of the temperature can be distinguished from the convoluted and the deconvoluted forms of the thermal contributions to the charge density as dynamic (DMD) and static multipole deformation (SMD) maps. The SMD maps offer a chance to compare the electron densities without the disturbance of the thermal vibration of atoms. Hence, the SMD maps have been computed and are presented in Figs. 5a – c for Al, Ni, and Cu, respectively.

3. Results and Discussion

The fitted profiles of the Rietveld refinements (Figs. 1a – c) for Al, Ni, and Cu, respectively) give a clear picture of the quality of the sample as well as of the data. The accuracy of the refinements can be judged from the difference curve between the observed and the calculated intensity, which is almost a straight line. The results of the structural refinement [3] given in Table 1 show reasonable values of the Debye-Waller factor for Al, Ni, and Cu obtainable from a powder data set, which is comparable to those reported in [21]. The experimental cell parameters of Al, Ni, and Cu are given in Table 1 and the differences from the reported values are 0.3 pm, 0.3 pm, and 9.6 pm for Al, Ni, and Cu, respectively [22], which are very small indicating the accuracy of the refinements and also the precision of the observed data sets. The reliability indices for all the powder samples are very small indicating the correctness of the refinements ($R_{\mathrm{P}} = 9.84\%$, 6.21%, and 6.77% for Al, Ni, and Cu, respectively).

The MEM electron density distribution map of Al as given in Fig. 2a for the (100) plane reveals the core of the Al atom being spherical and this sphericity persists even at slightly larger distances away from the centre. The distribution of the charges all over the plane indicates the distribution of the electrons while the charges at the edge centres in the (100) plane show the distribution of the perpendicular face-centered atoms, indicating the extension of the spread of the charges. The electron density map of Al in the (110) plane shows (Fig. 2b) highly concentrated charges at the core of the atoms and the distribution of the charges on places other than the atomic positions, due to the valence and the free electrons.

The cores of the Ni and Cu atoms as seen from the electron density map in the (100) plane (Figs. 2b, c), show the perfect spherical nature of the electronic charge clouds. The edge centres show the distribution of the electron density of the atoms located at the face centres of the planes perpendicular to the paper. Since the atomic numbers of Ni and Cu are higher than

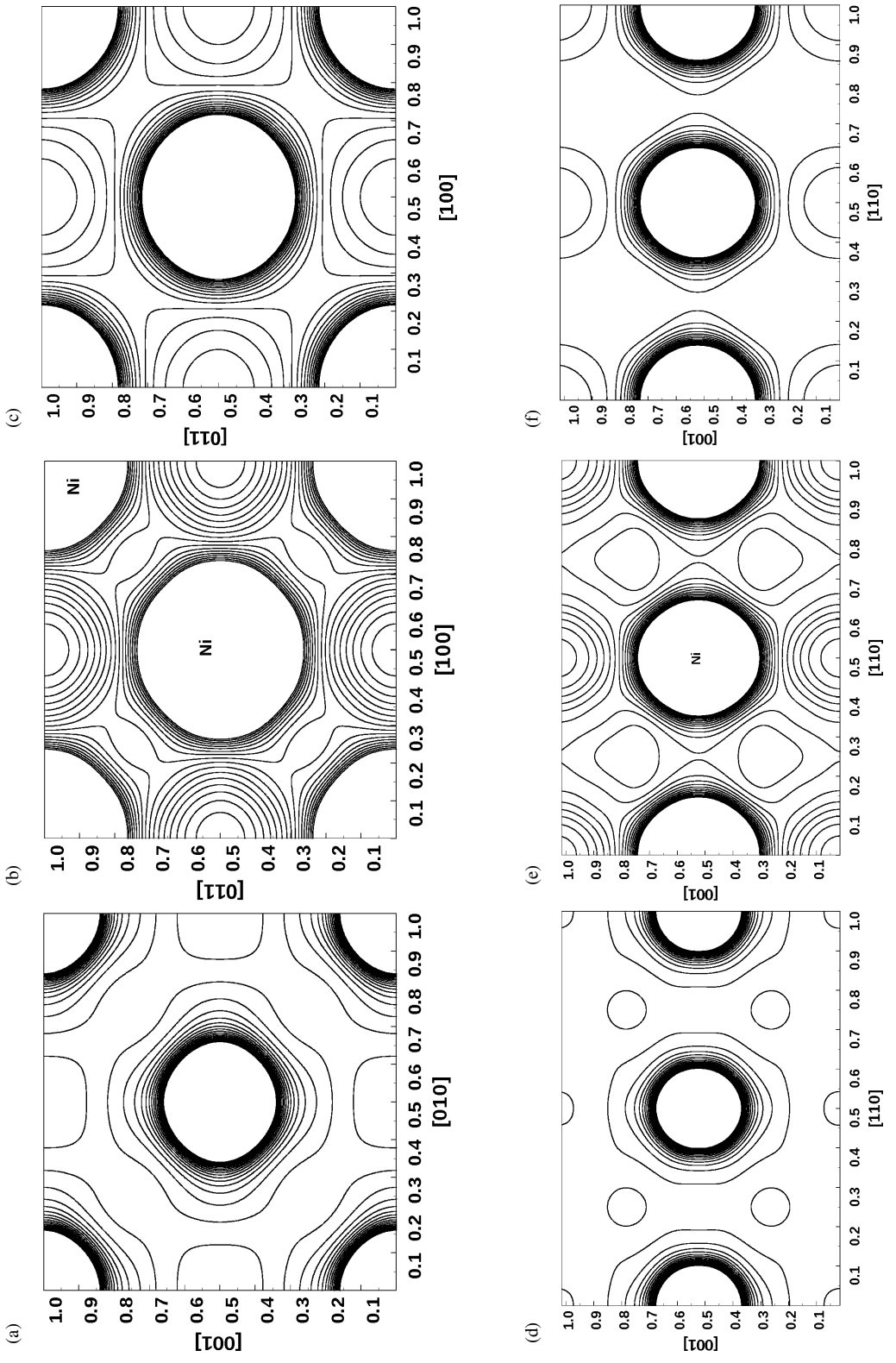

Fig. 2. (a) The MEM electron density distribution of Al in the (100) plane. The contour range is 0.0 to $2.0 \cdot 10^{-3}$ e/nm^3 and the contour interval is $0.1 \cdot 10^{-3}$ e/nm^3 for Fig. 2a – c. (b) The MEM electron density distribution of Ni in the (100) plane. (c) The MEM electron density distribution of Cu in the (100) plane. (d) The MEM electron density distribution of Al on the (110) plane. The contour range is 0.0 to $3.0 \cdot 10^{-3}$ e/nm^3 and the contour interval is $0.15 \cdot 10^{-3}$ e/nm^3 for Fig. 2d – f. (e) The MEM electron density distribution of Ni in the (110) plane. (f) The MEM electron density distribution of Cu in the (110) plane.

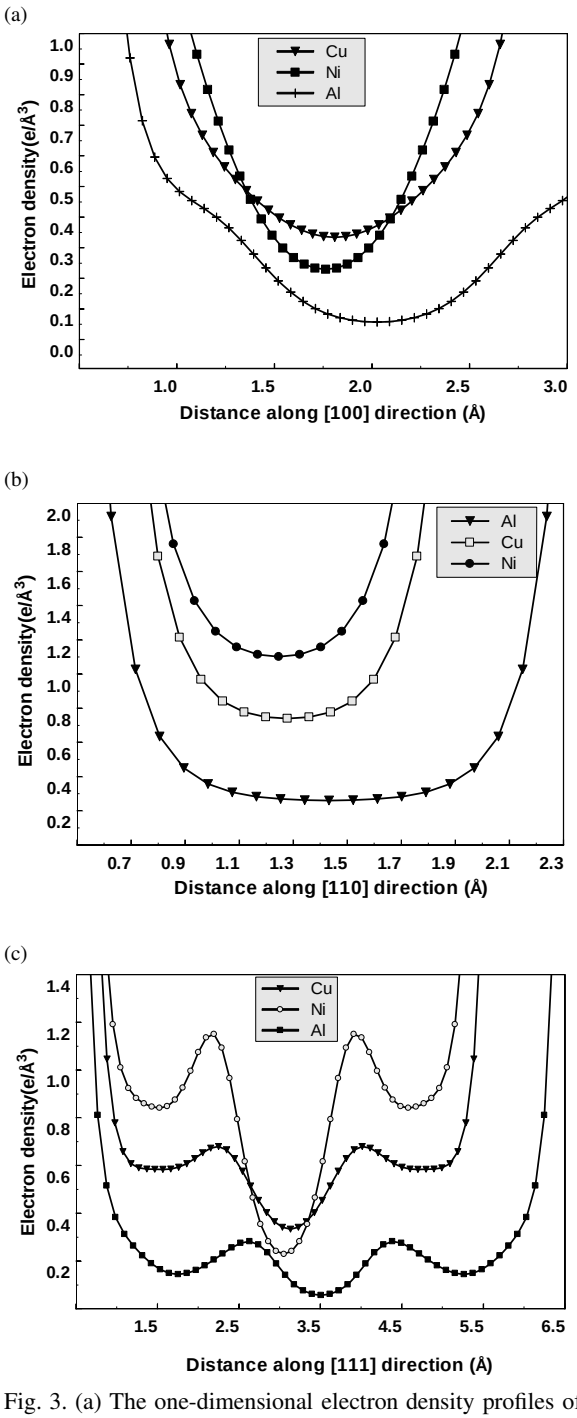

Fig. 3. (a) The one-dimensional electron density profiles of Al, Ni, and Cu along the [100] direction of the unit cell. (b) The one-dimensional electron density profiles of Al, Ni, and Cu along the [110] direction of the unit cell. (c) The one-dimensional electron density profiles of Al, Ni, and Cu along the [111] direction of the unit cell.

that of Al, a more diffuse distribution of charges is seen in the electron density maps of Ni and Cu in the (100) plane. The electron density maps of Ni and Cu in the (110) plane (Figs. 2e, f), show similar trends as observed in the (100) plane.

The one-dimensional profiles of the electron density constructed along the [100], [110] and [111] directions for Al, Ni, and Cu are shown in Figs. 3a – c, respectively. The positions of the minimum electron densities and the density values themselves given in Table 6. The mid-bond density for Al is found to be $0.264 \cdot 10^{-3}$ e/nm^3 at a distance of 0.1433 nm along the bonding direction [110]. The mid-bond electron density between the Al atoms along the [100] direction is $0.147 \cdot 10^{-3}$ e/nm^3 at a distance of 0.2026 nm. The first minimum and the mid-bond electron density between the atoms along the [111] direction are $0.119 \cdot 10^{-3}$ e/nm^3 and $0.147 \cdot 10^{-3}$ e/nm^3 at distances of 0.1755 nm and 0.3509 nm, respectively.

The mid-bond density for Ni is found to be $1.101 \cdot 10^{-3}$ e/nm^3 at a distance of 0.1247 nm along the bonding direction [110]. Table 6 shows that the mid-bond density along the [100] direction of Ni occurs at a distance of 0.1763 nm with a value $0.230 \cdot 10^{-3}$ e/nm^3. The first and second minimum electron density between the atoms along the [111] directions are $0.841 \cdot 10^{-3}$ e/nm^3 and $0.230 \cdot 10^{-3}$ e/nm^3 at distances of 0.1527 nm and 0.3054 nm.

The mid-bond density for Cu is found to be $0.765 \cdot 10^{-3}$ e/nm^3 at a distance of 0.1282 nm along the bonding direction [110]. The mid-bond density along the [100] direction occurs at a distance 0.1813 nm with a value $0.332 \cdot 10^{-3}$ e/nm^3. The first and second minimum electron densities between the atoms along the [111] direction are $0.664 \cdot 10^{-3}$ e/nm^3 and $0.332 \cdot 10^{-3}$ e/nm^3 at distances of 0.1374 nm and 0.3139 nm, respectively. The mid-bond density for Ni is the largest one (Table 6) among the three metals studied. But along the [100] and [111] directions (nonbonding), the element with higher atomic number has higher electron density. Hence, obviously the bonding interaction is stronger in Ni as is evidenced by the higher electron density along the [110] direction.

Hence, from the qualitative and quantitative analysis of the MEM electron densities, the bonding in Al, Ni, and Cu is predicted to be predominantly metallic and the interaction of the charges along other nonbonding directions for Ni, and Cu seems to be larger due to the metallic nature. (If the systems were ionic, one cannot expect higher mid-bond densities as in the present

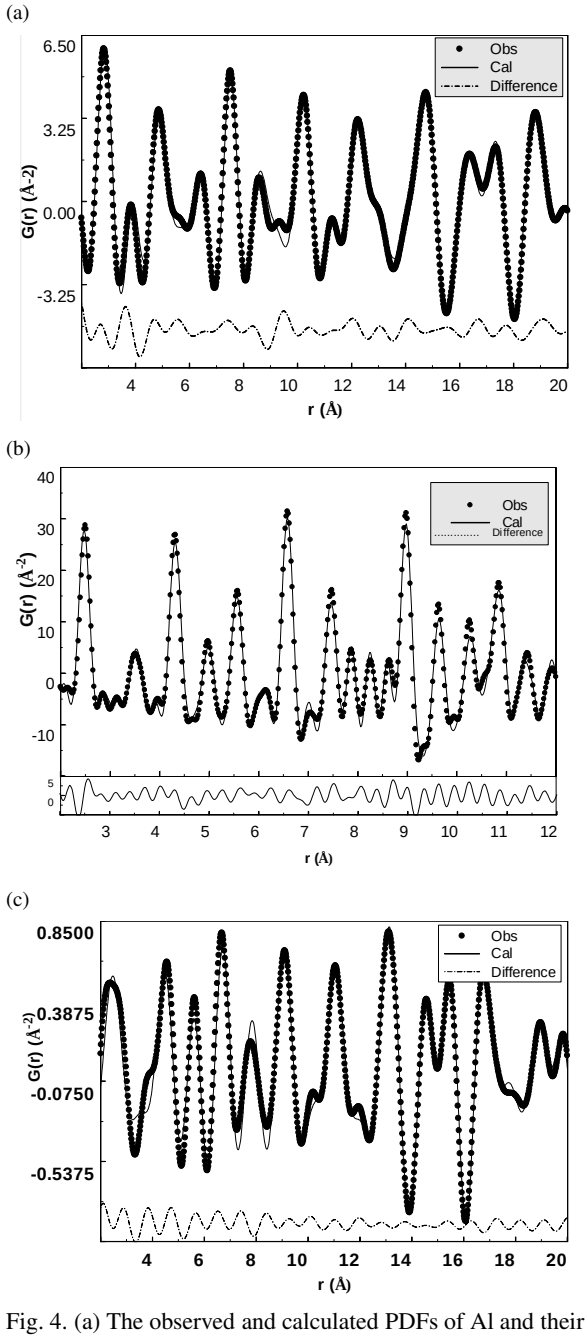

Fig. 4. (a) The observed and calculated PDFs of Al and their difference. (b) The observed and calculated PDFs of Ni and their difference. (c) The observed and calculated PDFs of Cu and their difference.

cases, and if the systems were covalent, one can expect values higher than the present values due to overlapping of charges.) Also the strength of the electron density is larger in the case of Ni, which has a smaller number of electrons in the unit cell compared to Cu. The electron density of Al in all three directions [100], [110], and [111], is relatively low compared to Ni and Cu, which reveals the loosely packed electron density of Al. (The interaction of the atomic charges will be less and hence the electron densities along the bonding and in directions other than the bonding one are expected to be minimum.)

The refined pair distribution functions [the Fourier transforms of $S(\vec{Q})$, the reduced structure factors] given in Figs. 4a – c for Al, Ni, and Cu show good matching of the observed and calculated PDFs. The PDF refinement can be considered as equivalent to the matching of the observed X-ray powder data with a model with too low structure parameters. Moreover, high Q data are required for this type of analysis on short-range order and local structure of materials [23]. In spite of these facts, an attempt has been made to use the X-ray powder data for this analysis too, to test how well these powder data sets can be used for purposes like a PDF analysis.

The peaks in the PDF profiles correspond to the nearest neighbour distances which are given in Table 7. In Al, the difference between the observed and the calculated first nearest neighbour distances turns out to be 0.0003 nm. In Ni, the corresponding difference is 0.0008 nm and for Cu it turns out to be 0.0184 nm, respectively. These differences are small considering the fact that we have used only (i) powder data with (ii) limited Q values. There may be local undulations in the structure of these three systems also, which lead to these differences. The local disorder is expected to affect the repetition distances, because of the diffuse scattering, which does not have a sharp, single pointed X-ray diffraction phenomenon. Hence, it is reflected in the local structur of analysis using suitable tools like PDF. From these differences, one can conclude that (i) the local disorder increases as the atomic number increases due to a higher concentration of charges, and (ii) the disorder propagates to a longer distance from the origin leading to enhanced differences in the neighbour distances. In the case of Cu, an additional disorder is possible due to the fact that Cu Kα, radiation has been used for collecting the powder data, which gives rise to resonance effects and possibly fluorescence.

The PDF profile of Ni has been compared with that obtained by Proffen and Billinge [19]. One can observe a very close resemblance among these two refinement results. The R values are also close to each

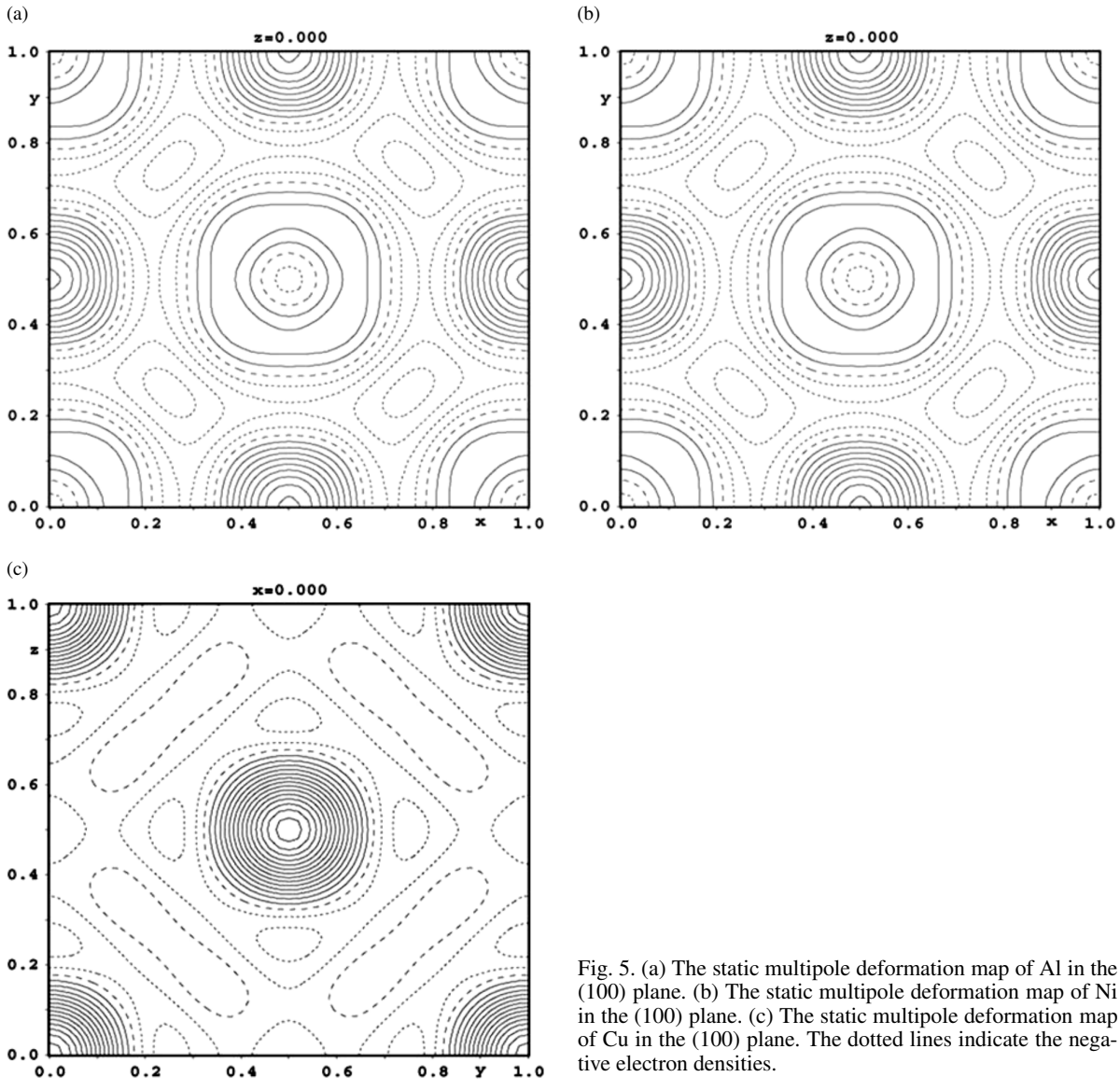

Fig. 5. (a) The static multipole deformation map of Al in the (100) plane. (b) The static multipole deformation map of Ni in the (100) plane. (c) The static multipole deformation map of Cu in the (100) plane. The dotted lines indicate the negative electron densities.

other (18% in the present work compared to 14% in the work by Proffen and Billinge [19]).

The multipole refinement shows no expansion/contraction for Al as seen from the κ' value given in Table 8 [$\kappa' = 1.007(0.052)$]. In the case of Cu, there is a slight contraction of the atom, but in Ni there is appreciable contraction compared to the other two systems. There is a possibility that the contraction is effected by obeying Pauli's principle which make that system stable, which has the strongest mid-bond interaction (as evidenced by the mid-bond electron density of Ni).

The results of the SMD calculations are given in Table 8, in which the positive and negative (maximum and minimum) electron densities are listed for all the three systems. Since these calculations are based on density differences, the smallest electron densities are seen for all these systems, i. e., the maximum positive difference is $0.05 \cdot 10^{-3}$ e/nm^3 for Al and the maximum negative density is $-0.08 \cdot 10^{-3}$ e/nm^3 for Ni. These values indicate the accuracy with which the multipole analysis has been carried out. Moreover, the positive density differences are the same both for Ni and Cu ($0.02 \cdot 10^{-3}$ e/nm^3), thus justifying the fact that no bi-

ased results are obtained as far as the comparison of the electron densities of Ni and Cu is concerned.

4. Conclusion

In the present work a clear understanding of the structure of the metals A1, Ni, and Cu has been obtained in terms of the cell parameters, thermal vibrations and electron density distributions in the bonding region using the MEM and the local structural analysis using the PDF. The multipole model analysis reveals a clear qualitative and quantitative picture of the charge densities both in the core and the valence region with the expansion and contraction of the valence region.

[1] D. M. Collins, Nature **49**, 298 (1982).
[2] N. K. Hansen and P. Coppens, Acta Crystallogr. A **34**, 909 (1978).
[3] V. Petříček, M. Dušek, and L. Palatinus, JANA2000, The Crystallographic Computing System, Institute of Physics, Academy of Sciences of the Czech Republic, Praha 2000.
[4] P. Coppens and A. Volkov, Acta Crystallogr. A **60**, 357 (2004).
[5] R. D. Poulsen, A. Bentien, T. Graber, and B. B. Iversen, Acta Crystallogr. A **60**, 382 (2004).
[6] J. Frils, B. Jiang, J. Spence, K. Marthinsen, and R. Holmestad, Acta Crystallogr. A **60**, 402 (2004).
[7] S. Pillet, M. Souhassou, and C. Lecomte, Acta Crystallogr. A **60**, 455 (2004).
[8] D. Marabello, R. Bianchi, G. Gervasio, and F. Cargnoni, Acta Crystallogr. A **60**, 494 (2004).
[9] R. Saravanan, Y. Ono, M. Isshiki, K. Ohno, and T. Kajitani, J. Phys. Chem. Solids **64**, 51 (2003).
[10] S. Israel, R. Saravanan, and R. K. Rajaram, Physica B **349**, 390 (2004).
[11] S. Israel, R. Saravanan, N. Srinivasan, and R. K. Rajaram, J. Phys. Chem. Solids **64**, 879 (2003).
[12] S. Israel, R. Saravanan, N. Srinivasan, and R. K. Rajaram, J. Phys. Chem. Solids **64**, 43 (2003).
[13] T. Proffen and R. Neder, J. Appl. Crystallogr. **30**, 171 (1997).
[14] H. Toby and T. Egami, Acta Crystallogr. A **48**, 336 (1992).
[15] P. F. Peterson, E. S. Bozin, T. Proffen, and S. J. L. Billinge, J. Appl. Cryst. **36**, 53 (2003).
[16] P. Debay and H. Menki, Phys. Z. **31**, 797 (1930).
[17] B. E. Warren, X-Ray Diffraction, Addision-Wesley, New York 1969.
[18] D. T. Bowran and J. L. Finney, J. Chem. Phys. **118**, 8357 (2003).
[19] T. Proffen and S. J. L. Billinge, J. Appl. Cryst. **32**, 572 (1999).
[20] I. K. Jeong, J. Thompson, T. Proffen, A. Perez, and S. J. L. Billinge, PDFGetX, A Program for Obtaining the Atomic Pair Distribution Function from X-Ray Powder Diffraction Data, 2001.
[21] L. M. Peng, G. Ren, S. L. Dudarey, and M. J. Whelan, Acta Crystallogr. A **52**, 456 (1996).
[22] R. W. G. Wyckoff, Crystal Structure, Vol. I, Interscience Publishers, London 1963.
[23] T. Egami, JIM **31**, 163 (1990).